Efficient identification of inhibitors targeting the closed active site conformation of the HPRT from *Trypanosoma cruzi*

Douglas M Freymann[1], Mary Anne Wenck[2], Juan C Engel[3], Jun Feng[2], Pamela J Focia[2], Ann E Eakin[2,4] and Sydney P Craig III[2]

Background: Currently, only two drugs are recommended for treatment of infection with *Trypanosoma cruzi*, the etiologic agent of Chagas' disease. These compounds kill the trypomastigote forms of the parasite circulating in the bloodstream, but are relatively ineffective against the intracellular stage of the parasite life cycle. Neither drug is approved by the FDA for use in the US. The hypoxanthine phosphoribosyltransferase (HPRT) from *T. cruzi* is a possible new target for antiparasite chemotherapy. The crystal structure of the HPRT in a conformation approximating the transition state reveals a closed active site that provides a well-defined target for computational structure-based drug discovery.

Results: A flexible ligand docking program incorporating a desolvation correction was used to screen the Available Chemicals Directory for inhibitors targeted to the closed conformation of the trypanosomal HPRT. Of 22 potential inhibitors identified, acquired and tested, 16 yielded K_i's between 0.5 and 17 μM versus the substrate phosphoribosylpyrophosphate. Surprisingly, three of eight compounds tested were effective in inhibiting the growth of parasites in infected mammalian cells.

Conclusions: This structure-based docking method provided a remarkably efficient path for the identification of inhibitors targeting the closed conformation of the trypanosomal HPRT. The inhibition constants of the lead inhibitors identified are unusually favorable, and the trypanostatic activity of three of the compounds in cell culture suggests that they may provide useful starting points for drug design for the treatment of Chagas' disease.

[1]Department of Molecular Pharmacology and Biological Chemistry, Northwestern University School of Medicine, 303 E. Chicago Ave., Chicago, IL 60611, USA
[2]Laboratory of Molecular Parasitology and Drug Design, University of North Carolina School of Pharmacy, CB#7360, Chapel Hill, NC 27599-7360, USA
[3]Department of Anatomic Pathology, Tropical Disease Research Unit, San Francisco Veterans Administration Medical Center, 4140 Clement Street, San Francisco, CA 94121, USA
[4]Department of Biochemistry and Biophysics, University of North Carolina, School of Medicine, Chapel Hill, NC 27599-7360, USA

Correspondence: Sydney P Craig III
E-mail: scraig@unc.edu

Keywords: Chagas' disease; Hypoxanthine phosphoribosyltransferase; Structure-based drug design; *Trypanosoma cruzi*

Received: **14 June 2000**
Revisions requested: **19 July 2000**
Revisions received: **5 October 2000**
Accepted: **9 October 2000**

Published: **30 October 2000**

Chemistry & Biology 2000, **7**:957–968

1074-5521/00/$ – see front matter

PII: S1074-5521(00)00045-4

Introduction

Trypanosoma cruzi is the etiologic agent of Chagas' disease, which affects 16–18 million people in Latin America and more than 300 000 US immigrants [1–3]. Acute infection, often occurring in childhood, can lead to death by heart failure or meningoencephalitis, and chronic infection can lead to heart failure or the mega-syndromes affecting the esophagus or colon [1]. Currently only two drugs are recommended for treatment of Chagas' disease, Nifurtimox and Benznidazole [4]. These compounds kill the trypomastigote forms of the parasite circulating in the bloodstream and are effective in reducing many symptoms during the acute phase of infection, however, they do not completely eliminate the parasites and are relatively ineffective against the intracellular stage of the parasite life cycle. Treatment with either drug is complicated by serious toxic side effects, thus, new drugs for the treatment of Chagas' disease are urgently needed.

To identify potential target enzymes for structure-based inhibitor design, differences in host and parasite metabolism may be identified and exploited. One such difference exists between humans and protozoan parasites in the pathways for purine nucleotide biosynthesis. Unlike mammals, protozoan parasites do not possess the enzymes required for the de novo synthesis of purine nucleotides [5,6] and rely entirely on salvage pathways for the purine nucleotides needed in cellular metabolism [6]. In *T. cruzi*, the hypoxanthine phosphoribosyltransferase (HPRT; EC 2.4.2.8) is responsible for salvage of both hypoxanthine (Hx) and guanine bases from host nutrient pools for use in purine nucleotide synthesis [7,8]. This enzyme has been proposed as a target for antiparasite chemotherapy [5,9–11].

The HPRT catalyzes the transfer of a phosphoribosyl group from phosphoribosylpyrophosphate (PRPP) to a pu-

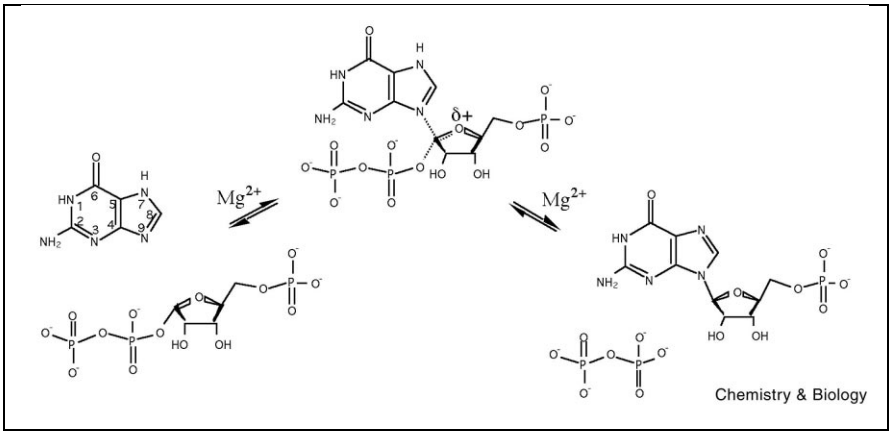

Figure 1. The reaction catalyzed by HPRT. HPRT catalyzes the reversible addition of 6-oxo-purines to the C1′ position of the ribose of PRPP. The reaction follows ordered bi–bi kinetics such that PRPP binds first, followed by the purine base and the product pyrophosphate is released before the product nucleotide [15,26,27]. There is evidence to support both S_N1 and S_N2 type chemistries [18,50,51].

rine base (Hx or guanine) to form a purine ribonucleotide, inosine monophosphate (IMP) or guanosine monophosphate (GMP), respectively (Figure 1). A number of apo, ion and product-bound HPRT crystal structures show disorder of a long active site loop (loop II, which contains invariant residues Ser81–Tyr82) [12–16], suggesting that the active site chemistry [17] is sequestered from bulk solvent by the formation of a 'closed' conformation of the flexible loop II not seen in these structures. The first structure with a closed and catalytically relevant conformation of the long flexible loop was that of the trypanosomal enzyme in ternary complex with the substrate PRPP and a substrate (Hx) analog [18]. In one subunit of the dimer, loop II is in a well-ordered closed conformation approximating that expected near the transition state. In the closed active site, the ternary substrate complex is almost completely protected from bulk solvent [18].

We reasoned that the closed active site would provide a favorable target for structure-based drug discovery. A common problem in docking ligands to proteins is that the target binding site is a fairly open surface, which effectively restricts the useful three-dimensional (3D) functionality of the ligand to interactions with a surface that, in the worst case, is little more than two-dimensional. An open active site further provides no restrictions on functionality extending into solvent, so that the computational search becomes less efficient due to many possible 'hits' that include large solvent exposed groups irrelevant to the predicted binding interactions. In the HPRT, closure of loop II completely defines a 3D space unique to the active site of the enzyme that can be exploited for structure-based drug design. The closed active site structure provides both a relatively restrictive target, which should result in more efficient identification of 'hits', and a well-defined 3D target volume surface that should maximize the information available to increase affinity and specificity of lead compounds.

Recent developments in molecular docking have addressed limitations caused by failure to allow flexibility of the interacting structures and by omission of a desolvation energy term in evaluating the energetics of binding to the target. The problem in the first case is that consideration of all possible conformations of both ligand and target can become computationally intractable. A protocol that simplifies and accelerates the evaluation of multiple ligand conformations has been implemented [19] and was used in this work. In this method, the conformational space of the database is simplified by expanding only over rotamers, and molecular docking is carried out in two stages, the first of which considers only the largest rigid fragment of each molecule. The result is a rapid, simple protocol that nevertheless allows evaluation of millions of conformations in the docking experiment. The problem in the second case is that of finding a reasonable approximation to account for the energetics of desolvation of both the active site and the ligand that accompanies binding. Such an expression has been identified [20] and is implemented in the program used here. Because it posits complete desolvation of the ligand on binding, this simple desolvation correction is particularly relevant to the case under consideration, in that closure of the active site of the HPRT should result in sequestration of the ligand from bulk solvent.

The modified version of the program DOCK [19–22] was used to screen an expanded database of over 34 million chemical structures for steric fit and predicted binding interaction with the closed active site structure of the HPRT from *T. cruzi*. A number of the computational hits were characterized biochemically and the majority of these compounds were found to inhibit the activity of the trypanosomal HPRT. In most cases, the kinetics of inhibition were consistent with the predicted binding mode. Of the molecules that inhibited the activity of the purified enzyme, three inhibited growth of trypanosomes in mammalian cell culture.

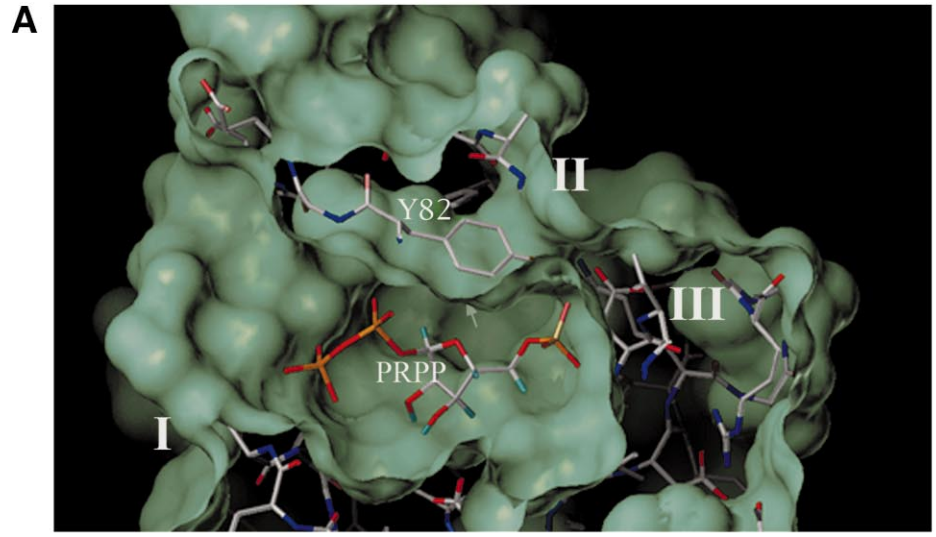

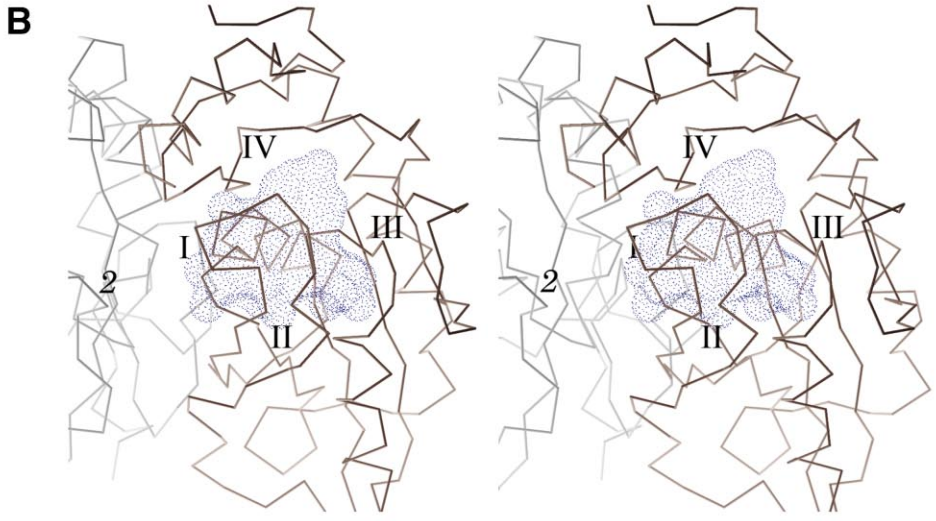

Chemistry & Biology

Figure 2. The active site of the HPRT in a closed conformation. **(A)** A cutaway view of the molecular surface of the active site of the closed conformation of the *T. cruzi* HPRT illustrating the position of the bound PRPP [18]. The view is through the flexible loop II, and a number of the atoms of that loop are cut away. The loops I and III at each side of the active site form hydrogen bonding interactions with the phosphate groups that position the PRPP, complexed with two magnesium ions, in a rigid conformation spanning the binding pocket. Deeper inside the pocket (indicated by the arrow) is the purine binding site that is formed by a cluster of hydrophobic side chains. The purine is buried in this view. Tyrosine 82 of loop II, center, is invariant. **(B)** A stereo view of the surface defined by the closed active site (dotted) in the context of an α carbon trace of the closed active site monomer. The orientation is rotated approximately 90° from that above. The surface is completely enclosed within the protein by the active site loops I–IV, by part of the second monomer of the dimer (indicated on the left), and by side chains which pack over the active site at the top right (not shown). The volume of the space enclosed by the surface is $\sim$610 Å^3; the area of the surface is $\sim$548 Å^2. This surface was the target for the DOCK screening described here.

Results

The closed active site target

The closed conformation of the *T. cruzi* HPRT encompasses an active site that spans approximately $11 \times 11 \times 7$ Å and encloses a volume of approximately 610 Å^3. In the crystal structure this space is entirely accounted for by well-ordered ligand atoms; these include the PRPP substrate, a purine substrate analog, two magnesium ions and a total of 14 water molecules (five of which are in the first coordination spheres of the two magnesium ions) [18]. Five

segments of the protein polypeptide backbone enclose the region: residues 50–53 (loop I), 79–85 (loop II), 111–120 (loop III), 163–165 and 169–173 (loop IV) (Figure 2A).

The interior of the closed active site is almost entirely inaccessible to bulk solvent (Figure 2B), with the exception of two small 'holes' at opposite ends of the active site that expose a total of approximately *22* Å^2, or ~4% of the surface area of the ligand ensemble, to the solvent. The purine binding pocket is largely hydrophobic and is created by four well-conserved side chains: Phe164 forms a π–π stacking interaction above the purine base, and Ile113 (loop III), Val165 and Leu170 (loop IV) sandwich it from behind and below. Neighboring main chain atoms interact with purine ring heteroatoms. The bound PRPP spans the binding pocket below the purine, with its 1′-pyrophosphate and 5′-phosphate groups interacting with residues of loop I and loop III, respectively, through backbone amide hydrogen bonds that stabilize the charged phosphate groups (Figure 2A). Two magnesium ions (termed M1 and M2) coordinate oxygen atoms of the PRPP pyrophosphate group. One magnesium (M1) has no direct interaction with the protein, while the other (M2) is coordinated by an invariant aspartate (Asp171) carboxylate oxygen. Thus, within the active site, there are different binding pockets characterized by distinct hydrophobic, hydrogen bonding and charged interactions.

DOCK screening calculations

The active site was prepared for DOCK screening by removing all 48 ligand atoms, including all ordered water molecules. The site shape was then described in terms of 55 DOCK spheres [23]. Although both will be addressed in future studies (see below), we did not define the shape of the site in terms of the ligand atomic positions [24], nor did we consider a number of 'structural' water molecules [25] observed in both the open and closed active sites of the *T. cruzi* ternary complex structure, as well as in a number of other HPRT structures with various ligands bound. The DOCK scoring grids were calculated over a 3D box that extended well beyond the enclosed active site in each dimension, in order to properly handle 'leakage' through the two small openings in the closed site. The scoring grids were calculated using the standard protocols for evaluation of van der Waals and electrostatic potential energies [22].

A conformationally expanded database of well over 34 million chemical structures [19] was then screened to assess potential fit and force field interactions with the closed active site (see Materials and Methods). The energy scores included a correction for ligand desolvation [20]. The top 500 compounds from the database search were considered for visual evaluation using computer graphics. The DOCK energy scores ranged from a minimum of −35.6 kcal/mol for the first to −23.7 kcal/mol for the 500th compound and followed a somewhat hyperbolic distribution characteristic

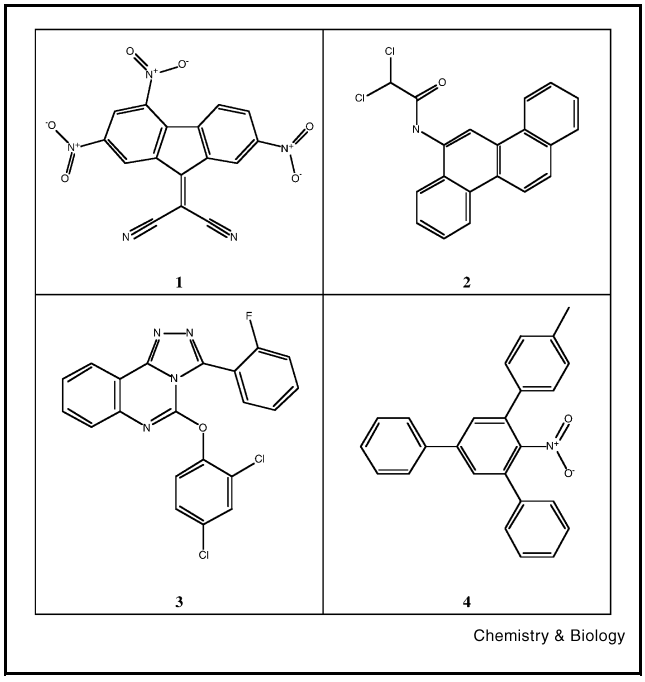

Figure 3. The four inhibitory compounds discussed in the text.

of DOCK scoring results. Over this range the relative energy scores have little meaning, and it is conventional to consider any of the top 500 compounds as candidates for further characterization [25]. A number of compounds were visually inspected for the plausibility of their predicted binding mode and for their likely solubility in aqueous media, and a subset of *22* compounds that minimized chemical redundancy was selected for initial kinetic characterization. The lowest scoring compound tested occurred third in the scoring list (score −30.9), and the highest occurred 389th (score −25.4); both proved to be low micro-molar inhibitors of the trypanosomal enzyme.

Predicted binding modes

We focus our discussion on four of the compounds identified in this study (Figure 3); their interactions can be taken as representative of the interactions of the other compounds identified in the DOCK screen. The predicted binding modes of the four compounds, which we identify as **1**, **2**, **3** and **4**, are shown in Figure 4. Each occupies from 300–370 Å^3 of the 610 Å^3 available volume of the HPRT binding pocket, generally within the broad central region of the site (see Figure 4). In the predicted binding orientations they interact with the pyrophosphate binding loop I, and each makes van der Waals interactions with Tyr82 of the closed flexible loop II. Both **3** and **4** present an aromatic ring to the hydrophobic purine binding pocket of the active site, wedged between, and forming van der Waals interactions with, residues Phe164 and Ile113. Phe164 is

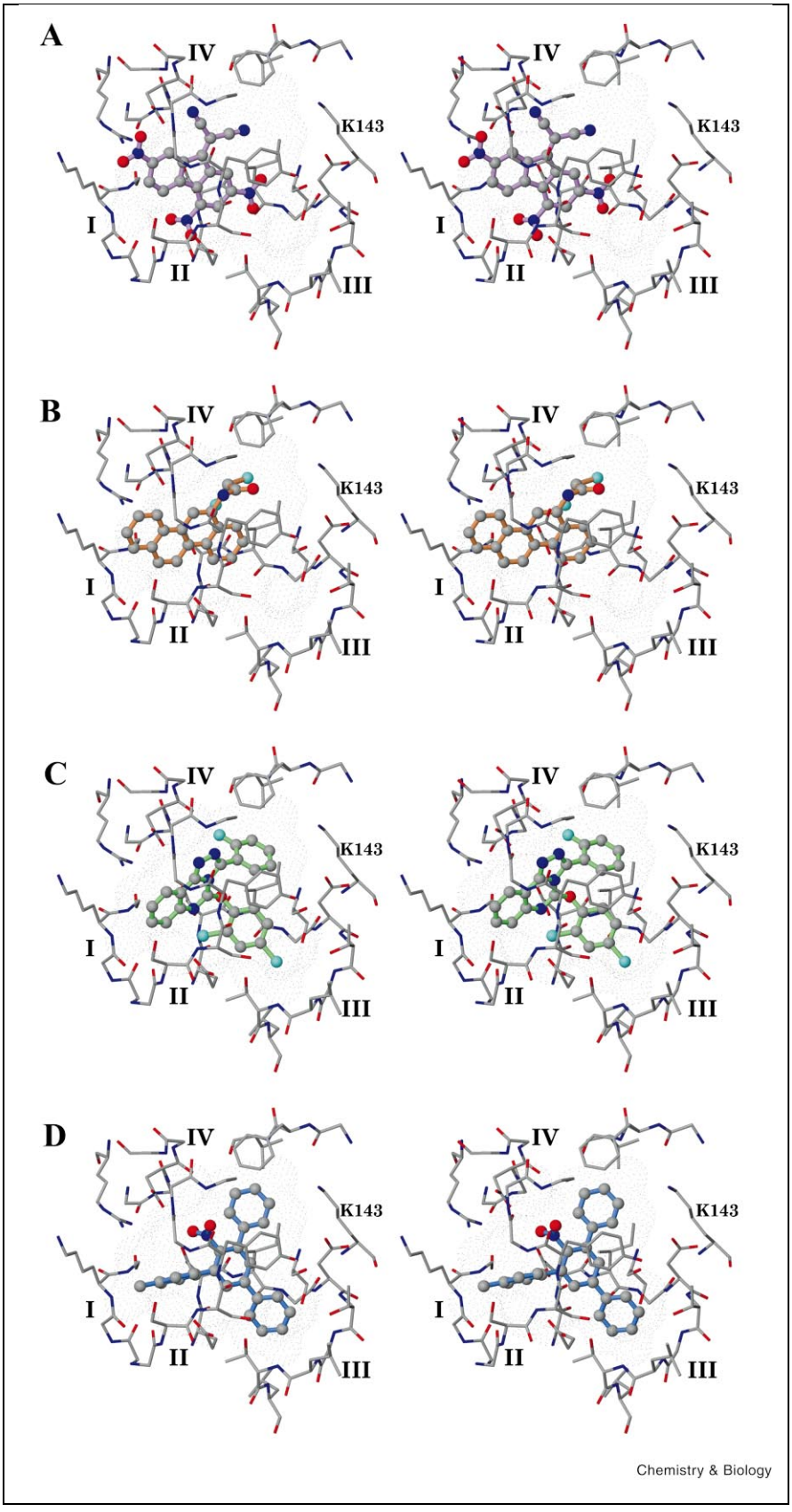

Figure 4. Predicted binding modes of four inhibitors identified by DOCK. Stereo images of the predicted binding modes of the four lead compounds (see text). The target DOCK surface is shown (dotted). The active site loops (I–IV) are indicated; side chains are drawn only for those residues that directly contact the active site ligand cluster. **(A)** Compound **1**, **(B)** compound **2**, **(C)** compound **3**, **(D)** compound **4**. The orientation is similar to that in Fig. 2B.

Figure 5. Inhibition kinetics. Lineweaver–Burke plots of initial velocity for different concentrations of each of the lead compounds (see text). The concentrations of inhibitor used were 0 μM (●), 0.625, 1.25, 2.5, 5 and 10 μM. In the plots labeled 'PRPP' (left), PRPP was the varied substrate, and in the plots labeled 'Hx' (right), Hx was the varied substrate. Given a sequential bi–bi reaction model, the pattern of inhibition of a compound that binds the empty active site should be competitive against the first substrate to bind (PRPP), and not competitive against the second substrate to bind (Hx) [28]. This is seen for compounds **1**, **2** and **4**. Compound **3** is uncompetitive with respect to PRPP. The insets show replots of the slopes for the three PRPP inhibition experiments that showed competitive behavior; these yield the derived inhibition constants.

→

known to be flexible, so that a π–π stacking interaction could easily occur. A fluorine atom of compound **3** (Figure 4C) is 2.9 Å from loop IV mainchain atoms in the purine binding pocket, and two chlorine atoms of the phenyl ring bound in loop III are predicted in a position that could contribute to van der Waals interactions as well. For compound **4** (Figure 4D), an NO_2 group is 2.8 Å from the polar environment of the Asp171 carboxylate. Compound **2** (Figure 3B) lacks an interaction with loop III and projects a smaller group that contains some polar atoms into the purine binding pocket. Finally, compound **1** (Figure 4A) is not predicted to bind extensively in either the purine binding pocket or loop III. Instead, this compound interacts primarily with loop I and occupies metal site M1, such that at least five atoms are within hydrogen bond distance to the sidechain of Asp171 and to mainchain atoms of Ile135 and the closed flexible loop II.

The contact that each of the compounds makes with Tyr82 can occur only in the closed conformation of the HPRT active site, and we believe it is significant that each of the compounds identified here exhibits some packing interaction with the closed flexible loop II. This is what distinguishes the result of the closed active site search from a search of the open active site. A DOCK search targeting the structure of the open monomer of the *T. cruzi* HPRT[18] has been carried out as well; the best force field score in that search was −24.6 kcal/mol, and all but that one score was worse than any compound scores reported in the closed active site search. A comparison of the predicted binding modes of the top 500 'hits' reveals that those targeted to the open active site cluster against the back wall of the active site, essentially the only surface defined in the target structure, while for the closed active site the distribution more fully explores the available space of the target volume, in particular, the space between loop I and the closed loop II that is predicted to contribute substantially to the binding interactions.

The compounds we have identified appear to complement the closed binding cavity well, although only a fraction of the 548 $Å^2$ of surface area available in the binding pocket is predicted to contribute to the van der Waals interaction energy with the ligands (which have surface areas of 279–348 $Å^2$). Those parts of the active site cavity not filled by the bound ligand may accommodate solvent molecules,

Table 1
Inhibition of the forward reaction of the HPRT from *T. cruzi*.

MDL-ACD[a]	Text reference	Variable PRPP		Variable Hx	
MFCD#		K_i (μM)	type[b]	$K^c_{i,app}$ (μM)	type
1159	***1***	***2.2***	***C***	***6.8***	***N-C***
5062		6.2	C	4.9	N-C
22291		*9.0*	*C*	*6.0*	*N-C*
32937		2.8	C	10.6	C
32980	*2*	*0.5*	*C*	*7.0*	*N-C*
37501		*3.3*	*N-C*	*21.8*	*N-C*
93980		*1.6*	*C*	*2.1*	*N-C*
112201		*7.9*	*C*	*4.4*	*C*
124181		2.1	C	3.0	N-C
139585		16.6	N-C	15.7	N-C
139586		5.9	C	5.6	C
141430	***3***	***11.8***	***U-C***	***10.6***	***C***
156385	***4***	***2.0***	***C***	***2.7***	***N-C***
170659		4.8	C	15.2	C
171313		4.4	C	33.9	N-C
189063		9.4	C	29.7	N-C

Compounds in *italics* were tested for activity against trypanosomes in culture; those shown in ***bold italics inhibit trypanosome growth.***
[a]MDL-ACD (the Available Chemicals Directory from MDL Information Systems) The full chemical name for each compound identified here by its MFCD # is given in Materials and Methods.
[b]C (competitive), N-C (non-competitive), U-C (uncompetitive).
[c]Measurements against variable Hx yield apparent inhibition constants ($K_{i,app}$)

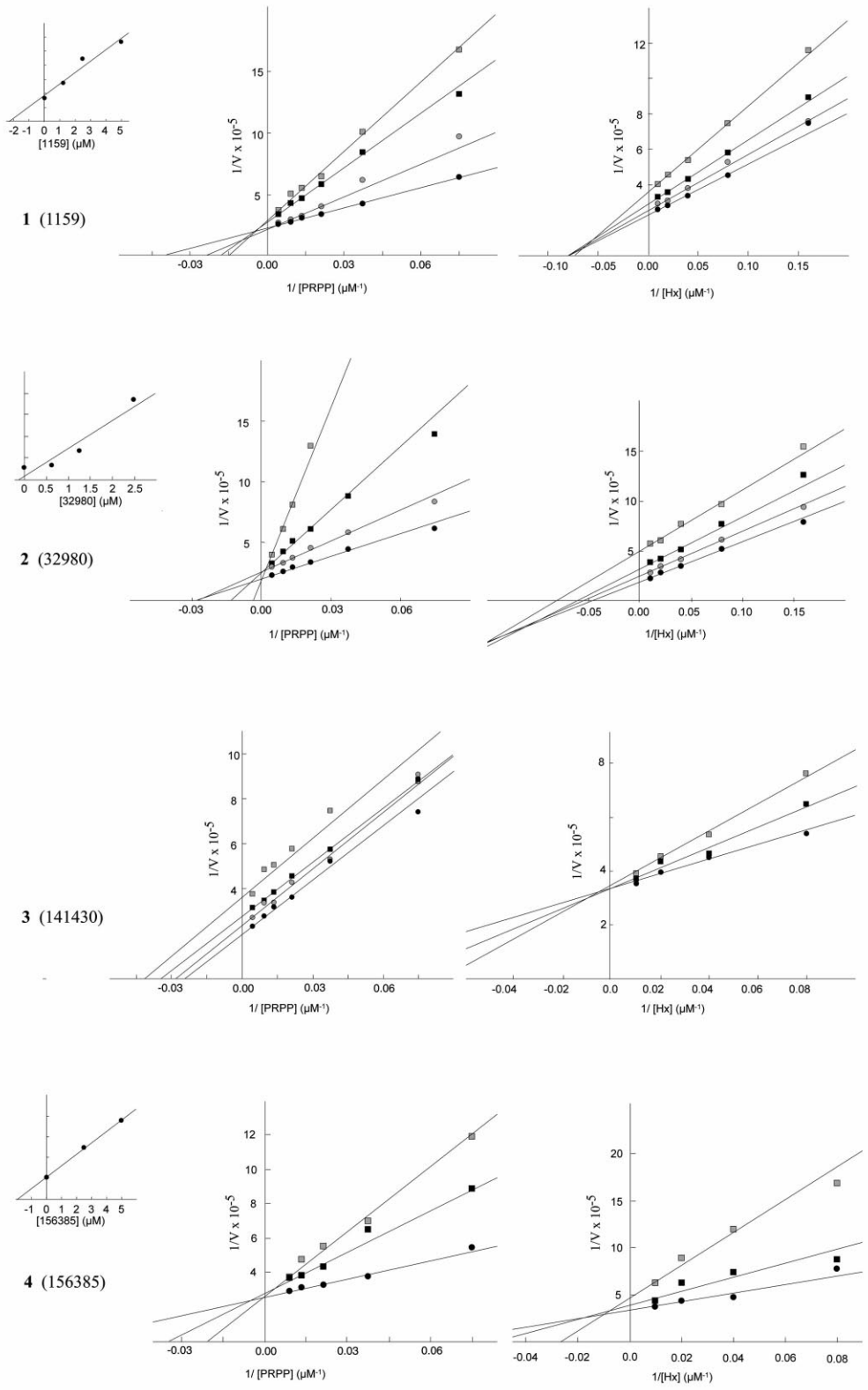
[1159] (μM)
1 (1159)
1/V x 10-5
1/ [PRPP] (μM-1)
1/ [Hx] (μM-1)
[32980] (μM)
2 (32980)
1/[Hx] (μM-1)
3 (141430)
[156385] (μM)
4 (156385)

and the predicted binding modes for a number of the compounds would allow several of the crystallographically observed water molecules to remain. Our inhibition kinetics data (below) are, in most cases, consistent with the computational binding predictions, however, a real understanding of the relation between the predicted binding modes and the actual binding modes awaits determination of the structures of each of the complexes.

Kinetic studies

Twenty-two compounds identified in the DOCK screen were acquired for biochemical characterization. Activity against the forward reaction of the HPRT was assayed using a continuous spectrophotometric assay [26]. In initial studies, 16 of the 22 compounds yielded IC_{50} values below 20 μM (data not shown); the inhibition activity of each of these compounds was then fully characterized (Figure 5 and Table 1). Thirteen of the 16 exhibited competitive inhibition kinetics against PRPP as the varied substrate, yielding inhibition constants (K_is) between 500 nM and 10 μM. The patterns of inhibition with Hx as the varied substrate were also determined for each of the 16 compounds (Table 1). Previous product inhibition [26,27], ligand binding, pre-steady state kinetics and isotope exchange [15] studies have demonstrated that the reaction mechanisms of the schistosomal, human and *Tritrichomonas foetus* HPRTs exhibit ordered bi–bi kinetics [28]. Given this framework we can ask whether the mode of inhibition observed in kinetic studies is consistent with the binding mode predicted in our computational screen. Indeed, the pattern of competitive and non-competitive inhibition against PRPP and Hx, respectively, that is seen with the majority of the compounds tested is consistent with a binding mode that competes with the first substrate (PRPP) for the open active site of the enzyme [28]. Four compounds were found to be competitive against *both* PRPP and Hx. This observation doesn't seem to be accommodated by a simple kinetic model given the predicted binding modes from DOCK, and it is not yet clear whether the results for these compounds reflect an ambiguity in the assay, or a true difference in the inhibitory or kinetic mechanism for the trypanosomal HPRT.

The three compounds that do not show competitive inhibition against PRPP are compound **3**, which was uncompetitive with PRPP and competitive with Hx, and compounds 37501 and 139585, which were non-competitive with both PRPP and Hx. The kinetics for inhibition by compound **3** are, however, consistent with the inhibitor binding to the protein after the substrate PRPP. We note that the *T. cruzi* HPRT is a dimeric enzyme, and that it is possible that binding to one active site could modulate the activity of the other [16]. With respect to compounds 37501 and 139585, closely related compounds 5062 and 139586 (differing in their lack of two chlorine atoms) were both competitive with the substrate PRPP. We do not yet have a rationalization for the behavior of these inhibitor pairs.

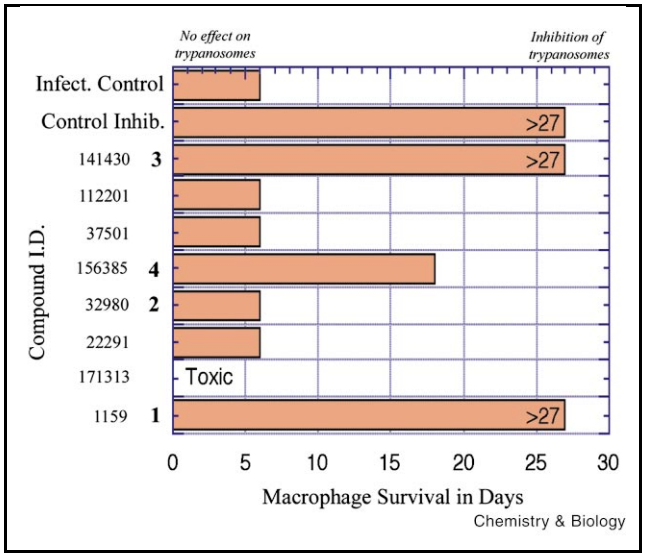

Figure 6. Inhibition of the growth of *T. cruzi*. Twelve of the 16 compounds listed in Table 1 were tested as inhibitors of the growth of *T. cruzi* in irradiated mouse macrophages. Four were insoluble. The eight remaining compounds were tested at a concentration of 10 μM. A cysteine protease inhibitor [30] was used as the positive control (Control Inhib.). Lead compounds **1** and **3** were as effective as the cysteine protease inhibitor in inhibiting parasite growth. In the absence of inhibitors, the first intracellular cycle of parasite replication was completed and infected macrophage cultures were virtually destroyed by 6 days after infection (Infect. Control). Tests were terminated after 27 days because irradiated macrophages survive for ≤ 30 days in culture.

Inhibition of trypanosomes in cell culture

Before pursuing further characterization of each of the inhibitors, we carried out preliminary tests of their effect on the growth of *T. cruzi*. Twelve of the 16 compounds that inhibited the purified HPRT were assayed, initially by measuring the growth of *T. cruzi* in infected mouse macrophage cultures in the presence of each of the compounds. Remarkably, of the eight compounds that remained soluble in media at 10 μM, three (**1**, **3** and **4**) inhibited the growth of parasites (Figure 6). Of the five other compounds, MFCD 171313 was toxic to the macrophages, and compounds **2** and MFCD 112201, 37501 and 22291 did not inhibit parasite growth. We note that four of five of the compounds that were ineffective in vitro possess potentially biologically unstable chemical groups (peptide bonds, an ester linkage or a reactive lactone ring).

Compound **3** was subsequently tested at 5 μM as an inhibitor of the growth of *T. cruzi* in infected human epithelial cells (Figure 7). Counts of the number of amastigotes per 50 infected cells in this experiment indicate that the

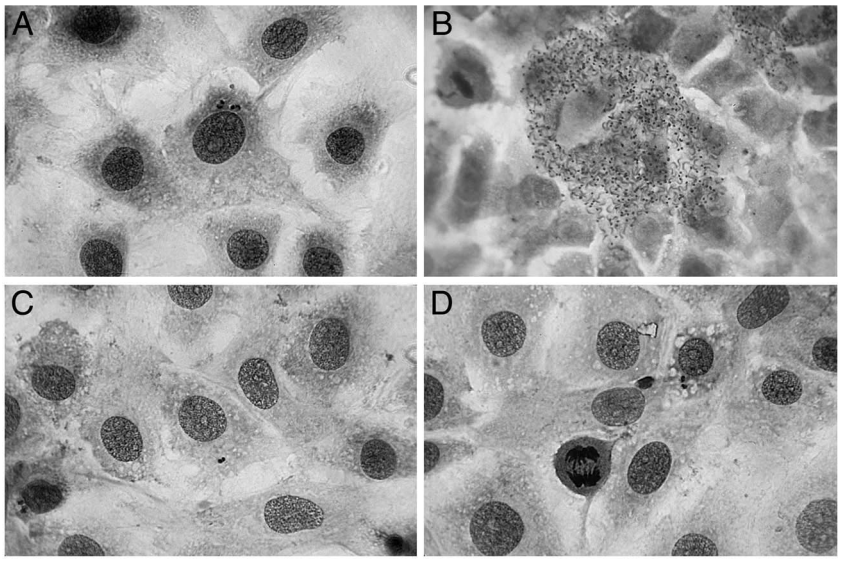

Figure 7. Human epithelial cells infected with *T. cruzi*. Inhibitor or DMSO control were added to human epithelial cell cultures 30 h after infection with a low titer of trypomastigotes. **(A)** Thirty h after infection amastigotes are visible in the cell in the center of the field of view. **(B)** Control cells, 6 days post infection. Two cells in this field of view are filled with differentiated trypomastigotes. **(C and D)** Infected cells in the presence of 5 μM compound **3**, 6 days post-infection. The mitotic figure in **(D)** is indicative of the low level of toxicity for compound **3**.

rate of replication of parasites in cells treated with compound **3** at 5 μM was more than seven-fold below that in control cells. Further, compound **3** exhibits low toxicity to human cells as indicated by the presence of mitotic figures in the epithelial cells after 6 days in the presence of the inhibitor (Figure 7).

Although these results establish that the compounds have an effect on trypanosome growth in culture, they cannot show whether or not the effect is mediated by the inhibition of the targeted enzyme, HPRT. As a first step towards addressing this question we asked whether increased levels of the normal substrate for the enzyme (Hx) had an effect on the inhibition observed. The inhibition of parasite growth by compounds **1** and **3** at 5 μM could be partially reversed by the addition of Hx to 300 μM in the media. Compounds **1** and **3** were also tested at 2.5 μM versus epimastigotes (insect stage parasites) in vitro. At these concentrations compound **3** killed approximately 20% of the parasites within 3 days. Compound **1** killed 100% of the parasites within 3 days, and its trypanocidal activity was largely reversed (88% survival) by the addition of Hx to 300 μM in the media.

Discussion

Of 22 compounds tested in the work described here, 16 inhibited the trypanosomal HPRT with inhibition constants between 0.5 and 17 μM. This remarkable efficiency of computational inhibitor discovery was likely due to the combination of a flexible ligand docking strategy that incorporated a desolvation correction, and the availability of the coordinates of the target enzyme in a well-defined closed conformation. In the absence of the flexible loop II, the open active site of the HPRT is a shallow solvent exposed cleft [29]; consequently the best HPRT inhibitor previously identified directly from a DOCK screen had an IC_{50} of 240 μM in a study targeting the purine pocket of the open active site of the *T. foetus* HGXPRT [29]. Our data show that the majority of the compounds identified in our DOCK screen targeting the closed active site of the *T. cruzi* HPRT are, in fact, inhibitors of the enzyme, and we find that the inhibition mechanism is generally consistent with binding to the targeted empty active site. Of the four compounds presented in Figure 3, three are trypanostatic in vitro (compounds **1**, **3** and **4**), and one is notable as a submicromolar inhibitor of the trypanosomal HPRT (compound **2**).

That these compounds, identified directly from the DOCK screen, should prove to have activity against live trypanosomes, and indeed, that two of them are as potent against trypanosomes in vitro as a cysteine proteinase inhibitor [30] presently in pre-clinical trials (James McKerrow, personal communication), is remarkable. We note that it has been a matter of controversy in the field whether the inhibition of the kinetoplastid HPRT should have an effect on growth at all [6,31,32]. In a related kinetoplastid, *Leishmania donovani*, separate HPRT and XPRT activities resolve to two phosphoribosyl transferase genes [32]; however, the same does not necessarily hold for *T. cruzi* as there are known differences in the activities of the purine salvage pathways of *Leishmania* and *T. cruzi* [33]. Our results, particularly the partial reversal of inhibition observed on addition of Hx, support an interpretation that the effect may be mediated by inhibition of the parasite HPRT activity. While the exact mechanisms of the inhibitors we have identified re-

main to be determined at both the structural and physiological levels, these results provide intriguing circumstantial evidence to support HPRT being a suitable target for the chemotherapeutic treatment of Chagas' disease.

Bearing these caveats in mind, we can nevertheless consider each of the compounds described here as potential leads for drug development. Each comprises a multi-ring system that occupies a similar molecular volume (ranging from ~300 Å^2 to ~367 Å^2) and, if the binding mode is as predicted computationally, each occupies a similar space in the target active site. Although the compounds are relatively hydrophobic, we note that the HPRT binding site is not uniformly hydrophobic and that the interactions in the predicted binding modes span the different functional regions of the site. Each of the compounds violates one (although only one) of Lipinski's 'rule of five' [34], a widely used indicator of poor absorption and permeation properties that provides a criterion for suitability as a drug. Thus, compound **1** has more than 10 H-bond acceptors (expressed as the sum of Ns and Os, 11 in this case), and compounds **2**, **3** and **4** have $C\log P$ values of 6.1, 6.5 and 6.8, respectively (all above the cutoff level of 5). To develop these compounds as specific inhibitors of the enzyme, several questions, of course, remain to be addressed. Although the DOCK calculations were carried out without consideration of the structural differences between the *T. cruzi* and human enzymes, it seems clear, given the predicted binding modes of the compounds, that there is ample space within the HPRT active site to elaborate functional groups that can exploit differences that do exist. A differential docking strategy has been used, for example, to identify selective inhibitors of DHFR [35], and our preliminary results suggest that the compounds already exhibit some selectivity for the trypanosomal enzyme relative to the human enzyme (data not shown). Second, we need structural confirmation of the binding modes of these compounds. Efforts are currently underway to determine crystal structures of the complexes of these compounds with the trypanosomal HPRT. Such structures should reveal the precise binding interactions between the compounds and the enzyme and should guide chemical modifications that improve binding specificity and pharmacological properties. Knowledge of the positions of bound solute molecules will allow improvement of the docking calculations (by specifying which waters, for example, are always present) and suggest directions in which to add functionality to increase affinity and specificity of lead inhibitors.

At this stage, however, we *can* state that we have identified a number of chemically unrelated inhibitors of the trypanosomal HPRT that inhibit the growth of *T. cruzi*. The purine auxotrophy of these protozoans remains a valid target for drug discovery, and whether the target proves to be one enzyme or several, our development of inhibitors for the HPRT is at least the first step, as the structure and chemistry of these families of enzymes are likely to be related; by exploiting the closed active site of the target our inhibitors in principle will exploit a common structural phenomenon. There are a large number of additional compounds in our DOCK screens that also have favorable energy scores but have not yet been biochemically characterized. Given the high hit rate of the compounds tested to date (16 of 22 yield K_is below 20 μM, and three of eight are trypanostatic) there are, therefore, likely to be many more potent inhibitors to be found among the compounds that scored well in the initial DOCK run. The closed active site structure of the trypanosomal HPRT has the potential to provide a productive system for the target-based development of inhibitory compounds that may lead to chemotherapy of disease caused by parasites.

Significance

We have identified a number of novel inhibitors of the HPRT by using a computational approach to target the closed active site structure of the trypanosomal enzyme. The DOCK screen was remarkably efficient, as 16 of 22 top scoring compounds were low micro-molar inhibitors of the target enzyme, and three of these compounds inhibited growth of trypanosomes in culture. The results of these preliminary studies suggest that the closed active site structure of the HPRT from *T. cruzi* provides an excellent target for inhibitor discovery. Furthermore, the trypanostatic activity of three of the inhibitors identified here provides support for the continuation of studies targeting inhibition of the HPRT as an approach to chemotherapy of Chagas' disease.

Materials and methods

Compounds

The name and commercial source of each compound that was purchased for testing is listed here with the MFCD identification number, provided by MDL Information Systems: 1159 (2,4,7-trinitro-9-fluorenylidenemalononitrile from ACROS, compound **1** in the text); 5062 (fluorescein diacetate, ACROS); 22291 (ethyl 6-bromo-dihydro-dioxo-4-methyl-7H-dibenzo(F,IJ)isoquinoline-1-carboxylate, Aldrich); 32937 (2,5-dinitro-9-(4-methoxyphenylimino)fluorene, Aldrich); 32980 (6-(2,2-dichloroacetamido)chrysene, Aldrich, compound **2** in the text); 36189 (eosin Y, ACROS); 37501 (2′,7′-dichlorofluorescein diacetate, ACROS); 93980 (2,7-dinitro-9-phenylcarbazole, Aldrich); 100793 (Maybridge); 102498 (Maybridge); 108271 (Maybridge); 112201 (Maybridge); 116399 (Maybridge); 124181 (Maybridge); 139585 (6-phenylimidazo[2,1-B] thiazole-5-carboxaldehyde-*o*-(2,6-dichlorobenzyl)oxime, Bionet); 139586 (6-phenylimidazo[2,1-B]thiazole-5-carboxaldehyde-*o*-(4-nitrobenzyl)oxime, Bionet); 141428 (3-(2-fluorophenyl)-5-(phenoxy)-1,2,4-triazolo(4,3-C)-quinazoline, Bionet); 141430 (3-(2-fluorophenyl)-5-(2,4-dichlorophenoxy)-1,2,4-triazolo(4,3-C)-quinazoline, Bionet, compound **3** in the text); 156385 (3,5-diphenyl-4′-methyl-2-nitrobiphenyl, Aldrich, compound **4** in the text); 170659 (Menai); 171313 (Aldrich); 189063 (Aldrich). When not specifically identified, MFCD numbers are used in the text.

Compounds were dissolved to 10 mM in dimethyl sulfoxide (DMSO) and stored at 4°C prior to use in inhibition assays. The purity of three of the lead compounds reported here (**2**, **3** and **4**) was confirmed by reverse phase high performance liquid chromatography. Compound **1** is light

sensitive and was found to degrade after several hours; this compound was used immediately upon making up the 10 mM solution.

Computational screening

The structure of the closed ternary substrate complex of the HPRT from *T. cruzi* (PDB ID: 1TC2) [18] was used to generate the target docking surface, after all active site ligands (PRPP, HPP, water and magnesium ions) were removed. Both monomers of the dimer were included during the calculations because one side of the targeted closed active site is defined by atoms of the other monomer. The molecular surface was generated using mass spectroscopy [36], and the binding site shape described in terms of 55 sphere centers generated using SPHGEN [23,37]. A maximum sphere radius of 4.5 Å, and a minimum radius of 1.4 Å, was used. The active site cluster positions were labeled as hydrogen bond donors and acceptors for chemical matching [38]. The DISTMAP grid was generated with default parameters over a $28.5\times 29.7\times 31.6$ Å box that extended well beyond the closed active site, and the force field scoring grid was generated by CHEMGRID [22] using default AMBER [39] parameters on a 0.3 Å grid with polar and nonpolar close cutoff limits of 2.3 and 2.8 Å, respectively. For calculations targeting the open active site, the open ternary substrate complex of the second monomer in 1TC2 was used. The binding site shape was described in terms of 58 sphere centers; other parameters were essentially as above.

Compounds were screened against the target site using a modified version of the program DOCK 3.5 [19–22]. The database used was conformationally expanded from the Available Chemicals Directory (the ACD from MDL Information Systems, San Leandro, CA, USA) so that up to 500 conformations for each structure in the ACD, a total of over 34 million conformations, were evaluated [19]. Solvation corrections were precalculated for each ligand and were included in the expanded database file [19,20]. Each ligand was matched to the target constellation of sphere atoms and screened for steric fit using the DISTMAP grid [40]. The DOCK bin sizes were 0.1 and 0.5 Å for ligand and receptor, respectively. Allowance was made in the initial fit for a single overlap with protein atoms. All orientations passing this criterion were then subjected to 10 cycles of minimization [41], and ligand interaction energy scores evaluated using the van der Waals and electrostatic potential distributions from CHEMGRID [22] and DELPHI [42]. Scoring included the correction for ligand desolvation [20]. The docking calculations required 10 days on a Digital Alpha 433au workstation.

High scoring compounds in the DOCK calculation were evaluated visually with respect to the active site structure using MIDAS-Plus [43] and O [44]. Nonpolar compounds were rejected from consideration, as were compounds with limited interaction with the binding site. Volumes were calculated using VOIDOO [45].

Enzyme kinetics

The HPRT from *T. cruzi* was purified from an overexpression system described previously [46]. Protein concentration was determined by Bradford assay using IgG as the standard. A continuous spectrophotometric assay [26] was used for HPRT activity studies and the determination of inhibition constants (see Table 1). Enzyme was pre-equilibrated with PRPP and inhibitor at 37°C for ≤30 s, and reactions were initiated by the addition of purine substrate. Production of IMP was monitored continuously by the change in absorbance at $\lambda = 245$ nm. The concentration of the enzyme in the reaction, 34.5 nM, was well below the concentrations of all other reactants.

For inhibition studies the concentration of either Hx ($K_M = 8.6$ μM) or PRPP ($K_M = 32.4$ μM) was held constant while the other substrate was varied. The concentration of Hx as the fixed substrate was 60 μM, while PRPP was varied between 13 and 215 μM. Alternatively, the concentration of PRPP was fixed at 67 μM, while Hx was varied between 6.25 and 100 μM. Initial velocity kinetics data were obtained for inhibitor concentrations between 625 nM and 20 μM. Inhibition was classified as competitive, noncompetitive or uncompetitive based on Lineweaver–Burke plots. Where appropriate, inhibition data were modeled as dead end inhibition of a sequential bi–bi system which, in the Lineweaver–Burke linearization of velocity data versus the first substrate yields slopes of:

$$\frac{K_{mA}}{V_{max}}\left(1+\frac{K_R}{[B]}\right)\left(1+\frac{[I]}{K_i}\right)$$

(where K_R is a ratio of kinetic constants, and K_i is the inhibition constant) [28]. For the determination of K_is, the apparent K_M and V_{max} at each inhibitor concentration were determined by non-linear regression assuming Michaelis–Menten kinetics. These values (K_M/V_{max}) were replotted against inhibitor concentration, and the K_i taken as the negative of the *x*-intercept of the least squares fit line [28]. Calculations were carried out using the program 'Enzyme Kinetics' from Exeter Software (Setauket, NY, USA).

Inhibition of parasite growth in culture

For cultivation and preparation of *T. cruzi*, a cloned population was derived from the Y strain [47]. This strain was cryopreserved in liquid nitrogen and axenically cultured epimastigotes were maintained in exponential growth phase by weekly passage in brain–heart infusion tryptose medium (BHT media) [48], supplemented with 20 μg/ml hemin and 10% (v/v) heat inactivated fetal bovine serum. Host cell lines (e.g. J774 mouse macrophage, IEC-6, BESM) were cultured in RPMI-1640 supplemented with 5% fetal calf serum at 37°C in a humidified atmosphere containing 5% CO_2. Trypomastigotes liberated from host cells were used to reinfect new cultures for serial maintenance of the parasites.

The protocols used for the in vitro assays of HPRT inhibitors were essentially as described [30]. Ten mM stock solutions of test compounds in DMSO were diluted with culture media and assayed at 5 or 10 μM. Culture media (with or without added inhibitor) was replaced three times per week to insure stable culture conditions and inhibitor levels. The effect of inhibitors on the intracellular amastigote stage was estimated by the lag time in the release of trypomastigotes in treated versus untreated cultures [49]. For experiments conducted at high infectivity in mouse macrophages the cells were irradiated (2400 rad) prior to infection in order to arrest their cell cycle.

Reversal of inhibition studies were carried out in triplicate. Six h after infection, inhibitor and Hx were added, and then every 24 h replaced with fresh media containing inhibitor and Hx. Cells were fixed and Giemsa stained 3 days after infection, and the total number of amastigotes per 100 infected macrophages counted. For assays of activity against epimastigotes, exponential phase epimastigotes were transferred to 25 cm^2 cell culture flasks containing 5 ml BHT media at a final concentration of 106 parasites/ml. Inhibitor and Hx were added at a final concentration of 2.5 and 300 μM, respectively, and after 3 days epimastigote survival was estimated by counting in a hemocytometer.

Acknowledgements

We thank David Lorber and Brian K. Shoichet for use of their developmental version of the program DOCK, developed partly through support from the NIH (GM59957 to B.K.S.). The ACD was provided by MDL Inc., San Leandro (to B.K.S.). This work was supported by NIH grants AI34326 (to S.P.C.III), AI38919 and AI45021 (to A.E.E.), and Northwestern University startup funds (to D.M.F.). We acknowledge the expert technical assistance of Mayur Desai and J. Ed Hall. D.M.F is a member of the Drug Discovery Program of Northwestern University.

References

1. Cook, G.C., ed. (1996). *Manson's Tropical Diseases*. W.B. Saunders, PA.
2. Panosian, C. (1998). The parasite of the poor. *Discover* **19**, 38–41.

3. Magill, A.J. & Reed, S.G. (2000). American Trypanosomiasis. In *Hunter's Tropical Medicine and Emerging Infectious Diseases*. (Strickland, G.T., ed.), 8th edn., pp. 653–664, W.B. Saunders, PA.
4. Morello, A. (1988). The biochemistry of the mode of action of drugs and the detoxification mechanisms in *Trypanosoma cruzi*. *Comp. Biochem. Physiol.* **90C**, 1–12.
5. Ullman, B. & Carter, D. (1995). Hypoxanthine-guanine phosphoribosyltransferase as a therapeutic target in protozoal infections. *Infect. Agents Dis.* **4**, 29–40.
6. Berens, R.L., Krug, E.C. & Marr, J.J. (1995). Purine and pyrimidine metabolism. In *Biochemistry and Molecular Biology of Parasites*. (Marr, J.J. & Muller, M., eds.), pp. 89–117, Academic Press, London.
7. Gutteridge, W.E. & Gaborak, M. (1979). A re-examination of purine and pyrimidine synthesis in the three main forms of *Trypanosoma cruzi*. *Int. J. Biochem.* **10**, 415–422.
8. Marr, J.J., Berens, R.L. & Nelson, D.J. (1981). Purine metabolism in *T. cruzi*. *Mol. Biochem. Parasitol.* **3**, 197–206.
9. Gutteridge, W.E. & Coombs, G.J. (1977). *Biochemistry of Parasitic Protozoa*, pp. 69–88, University Park Press, Baltimore, MD.
10. Dovey, H.F., McKerrow, J.H. & Wang, C.C. (1984). Purine salvage in *Schistosoma mansoni* schistosomules. *Mol. Biochem. Parasitol.* **11**, 157–167.
11. Craig III, S.P. & Eakin, A.E. (1997). Purine salvage enzymes of parasites as targets for structure based inhibitor design. *Parasitol. Today* **13**, 238–241.
12. Eads, J.C., Scapin, G., Xu, Y., Grubmeyer, C. & Sacchettini, J.C. (1994). The crystal structure of human hypoxanthine-guanine phosphoribosyltransferase with bound GMP. *Cell* **78**, 325–334.
13. Somoza, J.R., Chin, M.S., Focia, P.J., Wang, C.C. & Fletterick, R.J. (1996). Crystal structure of the hypoxanthine-guanine-xanthine phosphoribosyltransferase from the protozoan parasite *Tritrichomonas foetus*. *Biochemistry* **35**, 7032–7040.
14. Schumacher, M.A., Carter, D., Roos, D.S., Ullman, B. & Brennan, R.G. (1996). Crystal structures of *Toxoplasma gondii* HGXPRTase reveal the catalytic role of a long flexible loop. *Nat. Struct. Biol.* **3**, 881–887.
15. Xu, Y., Eads, J., Sacchettini, J.C. & Grubmeyer, C. (1997). Kinetic mechanism of human hypoxanthine-guanine phosphoribosyltransferase: rapid phosphoribosyl transfer chemistry. *Biochemistry* **36**, 3700–3712.
16. Focia, P.J., Craig III, S.P., Nieves-Alicea, R., Fletterick, R.J. & Eakin, A.E. (1998). A 1.4 Å crystal structure for the hypoxanthine phosphoribosyltransferase of *Trypanosoma cruzi*. *Biochemistry* **37**, 15066–15075.
17. Goitein, R.K., Chelsky, D. & Parsons, S.M. (1978). Primary ^{14}C and α secondary ^{3}H substrate kinetic isotope effects for some phosphoribosyltransferases. *J. Biol. Chem.* **253**, 2963–2971.
18. Focia, P.J., Craig III, S.P. & Eakin, A.E. (1998). Approaching the transition state in the crystal structure of a phosphoribosyltransferase. *Biochemistry* **37**, 17120–17127.
19. Lorber, D.M. & Shoichet, B.K. (1998). Flexible ligand docking using conformational ensembles. *Prot. Sci.* **7**, 938–950.
20. Shoichet, B.K., Leach, A.R. & Kuntz, I.D. (1999). Ligand solvation in molecular docking. *Proteins* **34**, 4–16.
21. Kuntz, I.D. (1992). Structure-based strategies for drug design and discovery. *Science* **257**, 1078–1082.
22. Meng, E.C., Shoichet, B.K. & Kuntz, I.D. (1992). Automated docking with grid-based energy evaluation. *J. Comp. Chem.* **13**, 505–524.
23. Kuntz, I.D., Blaney, J.M., Oatley, S.J., Langridge, R. & Ferrin, T.E. (1982). A geometric approach to macromolecule-ligand interactions. *J. Mol. Biol.* **161**, 269–288.
24. Tondi, D., Slomczynksa, U., Cosi, M.P., Watterson, D.M., Ghelli, S. & Shoichet, B.K. (1999). Structure-based discovery and in-parallel optimization of novel competetive inhibitors of thymidylate synthase. *Chem. Biol.* **6**, 319–331.
25. Shoichet, B.K. (1996). Docking ligands to proteins. In *Protein Structure Prediction: a Practical Approach*. (Sternberg, M.J.E., ed.), pp. 263–290, IRL Press, Oxford.
26. Yuan, L., Craig III, S.P., McKerrow, J.H. & Wang, C.C. (1992). Steady-state kinetics of the schistosomal hypoxanthine-guanine phosphoribosyltransferase. *Biochemistry* **31**, 806–810.
27. Munagala, N.R., Chin, M.S. & Wang, C.C. (1998). Steady-state kinetics of the hypoxanthine-guanine-xanthine phosphoribosyltransferase from *Tritrichomonas foetus*: the role of threonine-47. *Biochemistry* **37**, 4045–4051.
28. Segel, I.H. (1975). *Enzyme Kinetics*. Wiley, New York.
29. Somoza, J.R., Skillman, A.G.J., Munagala, N.R., Oshiro, C.M., Knegtel, R.M., Mpoke, S., Fletterick, R.J., Kuntz, I.D. & Wang, C.C. (1998). Rational design of novel antimicrobials: blocking purine salvage in a parasitic protozoan. *Biochemistry* **37**, 5344–5348.
30. Engel, J.C., Doyle, P.S., Hsieh, I. & McKerrow, J.H. (1998). Cysteine protease inhibitors cure an experimental *Trypanosoma cruzi* infection. *J. Exp. Med.* **188**, 725–734.
31. Gutteridge, W.E. & Davies, M.J. (1981). Enzymes of purine salvage in *Trypanosoma cruzi*. *FEBS Lett.* **127**, 211–214.
32. Jardim, A., Bergeson, S.E., Shih, S., Carter, N., Lucas, R.W., Merlin, G., Myler, P.J., Stuart, K. & Ullman, B. (1999). Xanthine phosphoribosyltransferase from *Leishmania donovani*. Molecular cloning, biochemical characterization, and genetic analysis. *J. Biol. Chem.* **274**, 34403–34410.
33. Berens, R.L., Marr, J.J., LaFon, S.W. & Nelson, D.J. (1981). Purine metabolism in *Trypanosoma cruzi*. *Mol. Biochem. Parasitol.* **3**, 187–196.
34. Lipinski, C.A., Lombardo, F., Dominy, B.W. & Feeney, P.J. (1997). Experimental and computational approaches to estimate solubility and permeability in drug discovery and development settings. *Adv. Drug Deliv. Rev.* **23**, 3–25.
35. Gschwend, D.A., Sirawaraporn, W., Santi, D.V. & Kuntz, I.D. (1997). Specificity in structure-based drug design: identification of a novel, selective inhibitor of *Pneumocystis carinii* dihydrofolate reductase. *Proteins* **29**, 59–67.
36. Connolly, M.L. (1983). Solvent-accessible surfaces of proteins and nucleic acids. *Science* **221**, 709–713.
37. DesJarlais, R.L., Sheridan, R.P., Seibel, G.L., Dixon, J.S., Kuntz, I.D. & Venkataraghavan, R. (1988). Using shape complementarity as an initial screen in designing ligands for a receptor binding site of known three-dimensional structure. *J. Med. Chem.* **31**, 722–729.
38. Shoichet, B.K. & Kuntz, I.D. (1993). Matching chemistry and shape in molecular docking. *Prot. Eng.* **6**, 723–732.
39. Weiner, S., Kollman, P., Case, D., Singh, U., Ghio, C., Alagona, G., Jr, S.P. & Weiner, P. (1984). A new force field for molecular mechanical simulation of nucleic acids and proteins. *J. Am. Chem. Soc.* **106**, 765.
40. Shoichet, B.K., Bodian, D.L. & Kuntz, I.D. (1992). Molecular docking using shape descriptors. *J. Comp. Chem.* **13**, 380–397.
41. Meng, E.C., Gschwend, D.A., Blaney, J.M. & Kuntz, I.D. (1993). Orientational sampling and rigid-body minimization in molecular docking. *Proteins* **17**, 266–278.
42. Gilson, M.K. & Honig, B.H. (1987). Calculation of electrostatic potentials in an enzyme active site. *Nature* **330**, 84–86.
43. Ferrin, T.E., Huang, C.C., Jarvis, L.E. & Langridge, R. (1988). The MIDAS display system. *J. Mol. Graph.* **6**, 13–27.
44. Jones, T.A., Zou, J.Y., Cowan, S.W. & Kjeldgaard, M. (1991). Improved methods for building protein models in electron density maps and the location of errors in these models. *Acta Cryst. A* **47**, 110–119.
45. Kleywegt, G.J. & Jones, T.A. (1994). Detection delineation, measurement and display of cavities in macromolecular structures. *Acta Cryst. D* **50**, 178–185.
46. Eakin, A.E., Guerra, A., Focia, P.J., Torres-Martinez, J. & Craig III, S.P. (1997). Hypoxanthine phosphoribosyltransferase from *Trypanosoma cruzi* as a target for structure-based inhibitor design: crystallization and inhibition studies with purine analogs. *Antimicrob. Agents Chemother.* **41**, 1686–1692.
47. Silva, L.H.P. & Nussenzweig, V. (1953). Sobre uma cepa de *trypanosoma cruzi* altament virulenta para o comondongo branco. *Folia Clin. Biol.* **20**, 191–203.
48. Cazzulo, J.J., Franke de Cazzulo, B.M., Engel, J.C. & Cannata, J.J.B. (1985). End products and enzyme levels of aerobic glucose fermentation in Trypanosomatids. *Mol. Biochem. Parasitol.* **16**, 329–343.
49. Harth, G., Andrews, N., Mills, A.A., Engel, J.C., Smith, R. & McKerrow, J.H. (1993). Peptide-fluoromethyl ketones arrest intracellular replication and intracellular transmission of *Trypanosoma cruzi*. *Mol. Biochem. Parasitol.* **58**, 17–24.
50. Shi, W., Li, C.M., Tyler, P.C., Furneaux, R.H., Grubmeyer, C., Schramm, V.L. & Almo, S.C. (1999). The 2.0 Å structure of human hypoxanthine-guanine phosphoribosyltransferase in complex with a transition-state analog inhibitor. *Nat. Struct. Biol.* **6**, 588–593.
51. Craig III, S.P. & Eakin, A.E. (2000). Purine phosphoribosyltransferases. *J. Biol. Chem.* **275**, 20231–20234.